APPLIED AND ENVIRONMENTAL MICROBIOLOGY, July 2004, p. 4222–4229 Vol. 70, No. 7
0099-2240/04/$08.00+0 DOI: 10.1128/AEM.70.7.4222–4229.2004

Osmotic Stress Response: Quantification of Cell Maintenance and Metabolic Fluxes in a Lysine-Overproducing Strain of *Corynebacterium glutamicum*

Cristian A. Varela, Mauricio E. Baez, and Eduardo Agosin*

Departamento de Ingeniería Química y Bioprocesos, Escuela de Ingeniería, Pontificia Universidad Católica de Chile, Santiago, Chile

Received 30 January 2004/Accepted 31 March 2004

Osmotic stress diminishes cell productivity and may cause cell inactivation in industrial fermentations. The quantification of metabolic changes under such conditions is fundamental for understanding and describing microbial behavior during bioprocesses. We quantified the gradual changes that take place when a lysine-overproducing strain of *Corynebacterium glutamicum* is grown in continuous culture with saline gradients at different dilution rates. The use of compatible solutes depended on environmental conditions; certain osmolites predominated at different dilution rates and extracellular osmolalities. A metabolic flux analysis showed that at high dilution rates *C. glutamicum* redistributed its metabolic fluxes, favoring energy formation over growth. At low dilution rates, cell metabolism accelerated as the osmolality was steadily increased. Flexibility in the oxaloacetate node proved to be key for the energetic redistribution that occurred when cells were grown at high dilution rates. Substrate and ATP maintenance coefficients increased 30- and 5-fold, respectively, when the osmolality increased, which demonstrates that energy pool management is fundamental for sustaining viability.

In industrial fermentations, increases in osmotic pressure, mostly a direct result of product accumulation, disrupt bacterial growth and the production of desirable compounds and may inactivate cells in many bioprocesses (26).

One strategy that microbes adopt to counteract higher osmotic pressure and to improve the likelihood of surviving such conditions is making use of organic intracellular solutes. Compatible solutes enable the cell to achieve osmotic balance without altering the cell's metabolic functions (35). The regulation of intracellular solute concentrations in response to the salinity of the medium provides the cell significant scope for adapting to changes in osmolality in the cell's environment (19).

Aside from altering compatible solute concentrations, the higher energy requirements for cell maintenance under osmotic stress also disrupt energy pool management (18). "Maintenance" covers every cellular reaction involving the consumption of ATP that does not contribute to the net synthesis of biomass. Such reactions include the need to build up and maintain steep ion concentration gradients across the membrane and macromolecular turnover (27).

Microbial growth and cellular productivity are driven by the flux balance generated between anabolic and catabolic reactions, as a higher osmotic pressure provokes numerous changes in the cell's metabolism. These fluxes vary considerably in response to changing environmental conditions (4, 34). Hence, a means for evaluating osmo-induced changes is necessary for the assessment and quantification of significant shifts within the metabolic network. Metabolic flux analysis is a powerful tool for quantifying such changes (22, 31–33).

Corynebacterium glutamicum is particularly appropriate for studying responses to osmotic stress, as this microorganism adapts efficiently to changes in osmotic pressure in the soil (6). It is also the most widely used microorganism for the industrial synthesis of amino acids (5). Although the physiological response of *C. glutamicum* to increases in osmotic pressure has been studied extensively, research has concentrated on individual pathways and not the organism's systemic response (7, 9, 10).

For this work, we applied metabolic flux balance analysis to assess and quantify the response of *C. glutamicum* ATCC 21253 to osmotic stress as well as to changes in the specific growth rate. We also evaluated how changes in osmotic pressures altered the substrate and ATP maintenance coefficients.

MATERIALS AND METHODS

Microorganism and medium. *C. glutamicum* ATCC 21253 was used throughout this study. In cultures with low levels of threonine, this strain overproduces lysine due to the bypassing of aspartate kinase inhibition by threonine plus lysine (12).

Initial seed cultures were grown in modified Luria-Bertani broth containing 10 g of tryptone liter^{-1}, 5 g of yeast extract liter^{-1}, 10 g of NaCl liter^{-1}, and 5 g of glucose liter^{-1}. A defined, threonine-growth-limiting medium was used for inoculation and reactor feeding (12).

Cultivation conditions. A 2-liter Braun Biostat B bioreactor with a 1.5-liter working volume was inoculated with 25 ml of microbial broth. The temperature was maintained at 30°C, and the pH was held at 7.0. Air was provided at a rate of 1 volume of gas per volume of liquid per min. The culture was grown in batch mode until the cell density approached the threonine limitation threshold. Constant feeding was then initiated at dilution rates of 0.21, 0.17, 0.13, and 0.09 h^{-1} by using a peristaltic pump. Each of these experiments was performed in duplicate. The osmolality of the culture was increased when a steady state was reached. It was increased linearly from 280 mosmol kg^{-1} up to 1,800 mosmol kg^{-1}, with the dilution rate kept constant by use of a second feed of the same medium supplemented with 1.2 M NaCl. The osmolality gradient lasted for 36 h. For each dilution rate, the total cultivation time (i.e., the time needed to reach steady-state conditions plus the time of the gradient) was short enough to avoid the appearance of revertants (11). The gradient continuous culture system was validated in an earlier study that compared continuous cultures with discrete osmolality values and gradient continuous cultures at the same dilution rate (34).

* Corresponding author. Mailing address: Pontificia Universidad Católica de Chile, Casilla 306, Correo 22, Santiago 782-0436 M, Chile. Phone: 562 354 49 27. Fax: 562 354 58 03. E-mail: agosin@ing.puc.cl.

Analytical techniques. Samples were taken periodically to determine the status of the fermentation. These were analyzed for osmolality, dry cell weight, glucose, trehalose, extracellular organic acids and amino acids, and ammonia, as described previously (34). Intracellular metabolites were extracted with a mixture of 1-bromohexadecane and 1-bromoheptane as a separation layer and $HClO_4$ as an acid fixation layer (13). This method significantly reduces contamination with external components. The oxygen uptake rate (OUR) and the carbon dioxide evolution rate (CER) were measured online as described elsewhere (8).

Stoichiometric model and metabolite balancing analysis. The stoichiometric model used to describe the metabolic network of *C. glutamicum* was described in earlier research (34). The stoichiometric matrix derived from the model has a condition number below 100, indicating that the estimated flux values are accurate even at relatively high measurement variances (27, 33). Appendix A lists every reaction used in the model.

The model assumptions were as follows. The respiratory chain of *C. glutamicum* is branched, with a variable efficiency depending on the growth conditions. During aerobic growth on minimal medium, however, the bc_1-aa_3 branch is the main operative branch. The transfer of two electrons from NADH to oxygen via this pathway results in the formation of 1.5 to 2 ATP molecules (1). Therefore, the P/O ratio (moles of ATP formed per oxygen atom) was considered constant throughout the saline gradient, with a value of 2. Two additional assumptions were made when we constructed the model. First, the macromolecular composition of the biomass (as shown in appendix A) was assumed to remain constant throughout the saline gradient; additionally, pyruvate carboxylase was the anaplerotic pathway considered in the network, since it has been reported as the major anaplerotic pathway of this microorganism (20, 21). Moreover, the flux through this anaplerotic pathway corresponds to the total anaplerotic flux, since metabolite balancing analysis cannot provide information about the size of each individual anaplerotic reaction flux.

The fluxes through the pathways of the bioreaction network were estimated from measurements of substrate uptake and product formation rates. Measurements and fluxes are connected through metabolite (stoichiometric) balances (33). Intracellular metabolite pools were assumed to be at a steady state, which is reasonable for continuous cultures.

Metabolite balancing analysis was performed to determine the flux distribution corresponding to each value of osmolality for each of the four different dilution rates.

Consistency analysis by integration of data for metabolic flux analysis. The substrate uptake and product formation rates of glucose, trehalose, organic acids (i.e., acetate, lactate, and pyruvate), and amino acids (i.e., alanine, valine, and lysine), in addition to the OUR, CER, and cell growth rate, were used to estimate metabolic fluxes. Based on the corresponding measurement variance, the relative standard deviations considered for the measured rates were as follows: for the CER, OUR, and ammonia, 10%; for trehalose, 8%; and for dry cell weight, glucose, organic acids, and amino acids, 5%.

Prior to any flux analysis, we checked to ensure that carbon balances accounted for at least 95% in every sample analyzed.

Nodal analysis. For nodal analysis, the fluxes around a particular metabolite node were depicted as normalized with respect to the total flux entering the node. A brief description of each of the nodes examined is given below.

(i) G6P node. Mass flows into the glucose-6-phosphate (G6P) node through the phosphotransferase system (equation A1 in appendix A) reaction, while the pathways consuming G6P are trehalose synthesis (A2), the pentose phosphate pathway (A23), glycolysis (A3), and biomass generation pathways (A33) that require G6P.

(ii) OAA node. Oxaloacetate (OAA) is produced from malate (A16) and replenished by the anaplerotic flux from the phosphoenolpyruvate/pyruvate (PEP/PYR) node. OAA is consumed from the aspartate aminotransferase (A31) and citrate synthase (A16) reactions.

Determining kinetic parameters. To determine substrate and ATP maintenance coefficients, we used the following equation:

$$r_i = Y^{\circ}_{xi}\,\mu + m_i \quad (1)$$

where i may be either the substrate or ATP. When metabolites are produced, however, the substrate maintenance coefficient (m_s) must be adjusted. To correct this, we used the method described by Stouthamer and van Verseveld (29) (see appendix B) and a theoretical substrate on product yield coefficient (Y°_{sp}) of 0.5 g g^{-1} (12). This method provides the maximum theoretically possible biomass on substrate yield (Y°_{sx}) and the substrate maintenance coefficient (m_s) as metabolites are produced. In this work, the latter coefficient was obtained by correcting the observed yield coefficient (m_s'), which represents the substrate needed to sustain both cell integrity and productivity (24). We then used the difference between the two coefficients ($m_s' - m_s$), which we called m_{sp}, to represent only the substrate necessary to sustain cell productivity.

TABLE 1. Modification of yield coefficients in response to rises in osmolality

Dilution rate (h^{-1})	Biomass yield on glucose (gDCW g^{-1}) at indicated osmolality (mosmol kg^{-1})			Lysine yield on glucose (gLys g^{-1}) at indicated osmolality (mosmol kg^{-1})		
	280	1,000	1,800	280	1,000	1,800
0.21	0.45	0.39	0.36	0.15	0.15	0.10
0.17	0.44	0.35	0.31	0.16	0.13	0.12
0.13	0.41	0.31	0.25	0.16	0.17	0.17
0.09	0.43	0.29	0.21	0.16	0.18	0.18

RESULTS

Response to osmotic stress. A series of continuous cultures of *C. glutamicum* with a saline gradient were developed in a chemical medium that was predetermined to promote lysine overproduction. Measurements were compared for each of the four dilution rates used (0.09, 0.13, 0.17, and 0.21 h^{-1}). The values for specific substrate consumption as well as for biomass and carbon dioxide production were higher at higher dilution rates.

For each of the dilution rates, the specific uptake of glucose increased linearly with the medium osmolality, although a higher rate of consumption was exhibited at lower dilution rates. At 0.09 h^{-1}, the specific glucose consumption increased twofold, while at 0.21 h^{-1}, the uptake increased by a factor of 1.2. Over the same period, a linear decrease in biomass production was observed for each dilution rate as the osmotic pressure increased. However, the decrease in biomass production was more dramatic at lower dilution rates. At 0.09 h^{-1}, the rate of biomass production was 57% lower than the initial rate, while at 0.21 h^{-1}, it only fell by 29%.

This behavior becomes clearer if we look at the change in the yield coefficient of biomass on glucose (Y_{sx}) with changes in the medium osmolality. For all of the dilution rates, the Y_{sx} values were similar as the saline gradient began (Table 1). As the osmolality increased, the yield coefficient fell. Once more, the reduction was higher at lower dilution rates, and at 0.09 h^{-1}, was half the initial value.

The main product of *C. glutamicum* ATCC 21253 is the amino acid lysine. The rate of lysine production at 0.21 h^{-1} increased moderately up to 800 mosmol kg^{-1} and then fell to below its initial value (34). This pattern was not repeated for the other dilution rates, all of whose lysine production rates increased linearly. Lysine production increased 2.2, 1.7, and 1.2 times for dilution rates of 0.09, 0.13, and 0.17 h^{-1}, respectively. The lysine yield on glucose was practically constant at 0.09 and 0.13 h^{-1}, while it decreased at both 0.17 and 0.21 h^{-1}, more markedly for the latter dilution rate (Table 1).

The accumulation of the main compatible solutes, trehalose and proline, occurred intracellularly and changed according to the medium osmolality and dilution rate. For dilution rates of 0.09 and 0.13 h^{-1}, the trehalose content rose almost linearly as the osmolality increased. For rates of 0.17 and 0.21 h^{-1}, on the other hand, trehalose increased up to 1,000 mosmol kg^{-1} and then

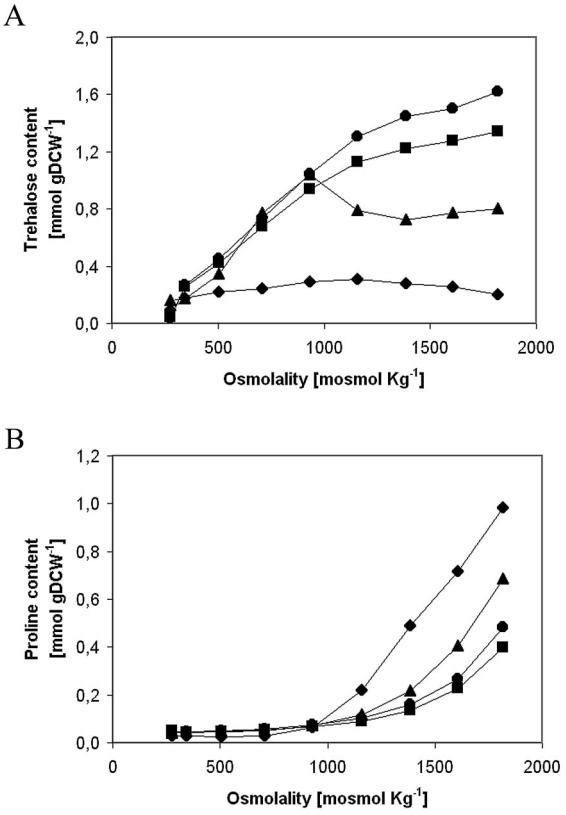

FIG. 1. Effect of medium osmolality on intracellular content at different dilution rates. The graphs show the intracellular accumulation of trehalose (A) and proline (B) at 0.09 h^{-1} (circles), 0.13 h^{-1} (squares), 0.17 h^{-1} (triangles), and 0.21 h^{-1} (diamonds).

decreased until the end of the gradient, at which point eight times more trehalose was accumulated for the 0.09-h^{-1} rate than for the 0.21-h^{-1} rate (Fig. 1A). Proline only started to be accumulated after an osmolality of 1,000 mosmol kg^{-1} was reached and rose to a maximum of 0.98 mmol g of dry cell weight $(gDCW)^{-1}$ for the dilution rate of 0.21 h^{-1}, which was almost two and a half times the content achieved for the 0.09-h^{-1} rate (Fig. 1B). Hence, trehalose is the principal osmolite throughout the gradient for dilution rates of 0.09 and 0.13 h^{-1}, while similar amounts of trehalose and proline were finally accumulated for the 0.17-h^{-1} rate. At 0.21 h^{-1}, however, more proline than trehalose was accumulated at high osmolalities.

Metabolic fluxes. Metabolic flux distributions across the network for the dilution rates of 0.09 and 0.21 h^{-1} at three different osmolalities are shown in Fig. 2. The fluxes were normalized with respect to the biomass formation rate, which facilitates a comparison of the outcomes of different osmolalities and dilution rates in the flux distribution map. Using biomass for normalization also makes possible the representation of fluxes such as the glucose phosphotransferase system.

As osmotic pressure rose, the consumption of glucose always increased for both dilution rates, although more so at 0.09 h^{-1}. The flux entering the metabolic network at 0.09 h^{-1} was directed to biosynthetic and degradation pathways that use G6P, specifically glycolysis, the pentose phosphate pathway, and trehalose production. At 0.21 h^{-1}, however, the flux was fed preferentially toward glycolysis (appendix A, equations A3 to A7).

At both dilution rates, the increased glucose consumption led to larger fluxes within the Krebs cycle (appendix A, equations A10 to A16); nevertheless, the 0.09-h^{-1} dilution rate attained higher values than the 0.21-h^{-1} rate. Identical behavior was observed for the flux directed to oxidative phosphorylation in response to higher NADH production, which triggers a rise in the production of ATP (equation A45).

For the 0.09-h^{-1} rate, as a result of the larger flux in the anaplerotic reaction that replenishes the OAA destined for the synthesis of lysine, fluxes forming aspartate and lysine increased linearly. For the 0.21-h^{-1} rate, on the other hand, the increased flux in this anaplerotic reaction was linked to the rigid PEP/PYR node and not to lysine production (34). The production of other amino acids, such as glutamine and valine, was also higher for 0.09 h^{-1} than for 0.21 h^{-1} (Fig. 2).

Nodal analysis. Information is essential for understanding the regulatory mechanisms of the cell in response to a particular stress. Nodal analysis aims to classify the nodes of the metabolic network based on their flexibility in coping with such stresses (28).

As osmotic pressure rose, the Embden-Meyerhof-Parnas (EMP)/pentose phosphate pathway ratio at the G6P node increased linearly for each of the four dilution rates (Fig. 3A). The ratio was lower for the rates of 0.09 and 0.13 h^{-1}, however, due to the higher reducing power needed to produce lysine.

PEP/PYR has been described as a rigid node under various conditions (28, 32), and we also observed this here (data not shown). As the glycolytic flux (the flux entering the node) increased, both the flux toward OAA and that toward the Krebs cycle rose proportionally.

The OAA node, which was described earlier as being flexible (34), varied in response depending on the dilution rate (Fig. 3B). At low rates of dilution (0.09 and 0.13 h^{-1}), the node was practically rigid, whereas at higher dilution rates it was flexible. Production was unaltered for rates of 0.09 and 0.13 h^{-1}, since the flux was constantly destined to the synthesis of aspartate, and later, lysine. For higher dilution rates, however, the tricarboxylic acid cycle/aspartate synthesis ratio rose with osmolality, thus privileging energy formation over lysine production.

Energetics and cellular maintenance. Figure 4 shows the rise in the observed maintenance coefficient on the substrate split into the carbon fraction needed to sustain cellular integrity and the fraction the cell requires for maintaining cell productivity. Both maintenance coefficients (m_s and m_{sp}) rose as the osmolality increased: m_s rose 30-fold (from 5 to 150 mg $gDCW^{-1}$ h^{-1}), while m_{sp} merely increased 10-fold (from 20 to 200 mg $gDCW^{-1}$ h^{-1}). In addition, we observed that Y_{sx} remained almost constant throughout, at 0.65 gDCW g^{-1}.

As the osmotic pressure rose in the medium, the carbon fraction used for maintenance (m_s/q_s) increased for every dilution rate and attained a maximum of 35% for 0.09 h^{-1} (Fig. 5). This fraction also varied depending on the dilution rate and was lower at higher rates of dilution. While less clearly discernible in the figure, the differences between the values for 0.09 and 0.21 h^{-1} reduced as the osmolality increased. At higher osmolalities, the rise in q_s was larger at lower dilution rates. The difference at 280 mosmol kg^{-1} was a factor of 2.2,

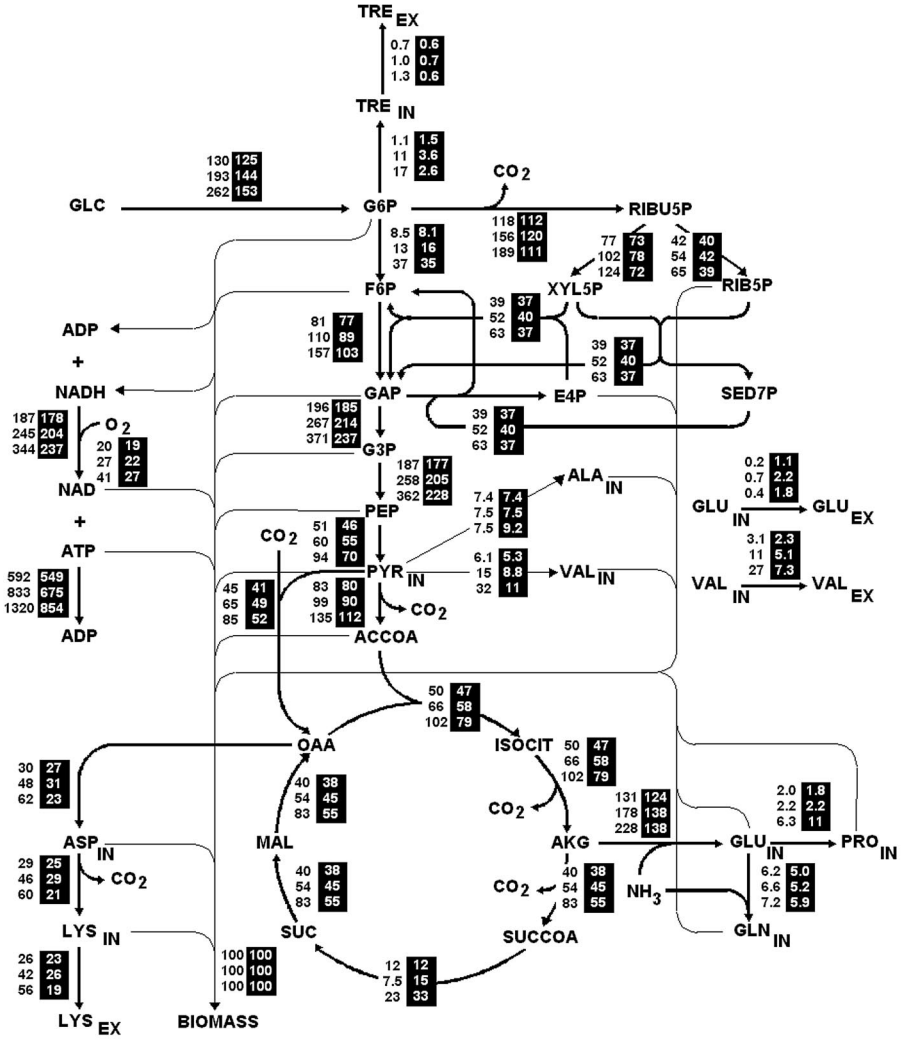

FIG. 2. Map of flux distributions at 0.09 h^{-1} (black numbers) and 0.21 h^{-1} (white numbers in black columns) at osmolalities of 280, 1,000, and 1,800 mosmol kg^{-1} (from top to bottom). The fluxes are expressed in millimoles per gDCW per hour and are normalized with regard to biomass formation. Abbreviations: TRE, trehalose; RIBU5P, ribulose-5-phosphate; F6P, fructose-6-phosphate; XYL5P, xylulose-5-phosphate; XYL6P, xylulose-6-phosphate; E4P, erythrose-4-phosphate; RIB5P, ribose-5-phosphate; SED7P, sedoheptulose-7-phosphate; GAP, glyceraldehyde-3-phosphate; G3P, glyceraldehyde-6-phosphate; ACCOA, acetyl-CoA; ISOCIT, isocitrate; AKG, α-ketoglutarate; SUCCOA, succinyl-CoA; IN, intracellular metabolite; EX, extracellular metabolite.

while at 1,800 mosmol kg^{-1}, the comparable difference in the carbon fraction used for maintenance fell to a factor of 1.4.

The ATP maintenance coefficient (m_{ATP}) rose linearly from 1.8 to 9.2 mmol $gDCW^{-1}$ h^{-1}, while Y_{xATP} remained almost constant, at 90 mmol $gDCW^{-1}$, as the osmolality increased.

DISCUSSION

Changes in the biomass yield coefficient in response to stresses in the medium demonstrate the cell's ability to adapt its metabolism in response to adverse conditions. Hence, the cell is only affected by changes in osmolality if this coefficient varies. *C. glutamicum* confronted osmotic stress better at higher specific growth rates since the biomass yield coefficient decreased only 20%.

At low dilution rates, lysine production increased, since under such conditions the bacterial metabolism speeds up. The rise in glucose consumption produced a higher level of lysine production, and the lysine-on-glucose yield coefficient remained constant throughout the saline gradient. The faster metabolism in turn led to more valine, trehalose, and proline biosynthesis.

Several microorganisms use a cocktail of osmolites in order to cope with changes in osmotic pressure (35). External conditions largely dictate which of the osmolites predominates within the cell (2, 14, 23). At low dilution rates, trehalose dominated throughout the gradient. Proline, however, was only significant at high osmolalities and high rates of dilution. The use of trehalose as a compatible solute has a higher energetic cost than the use of proline does (19). The cell improves its energy efficiency by changing the osmolite it uses at higher dilution rates and thus is better able to cope with higher osmotic pressures.

Unlike proline, trehalose is also found in the extracellular medium. The excretion of trehalose under conditions of low water availability (increased osmotic pressure or dehydration) has been reported for *Escherichia coli* and *Saccharomyces cere-*

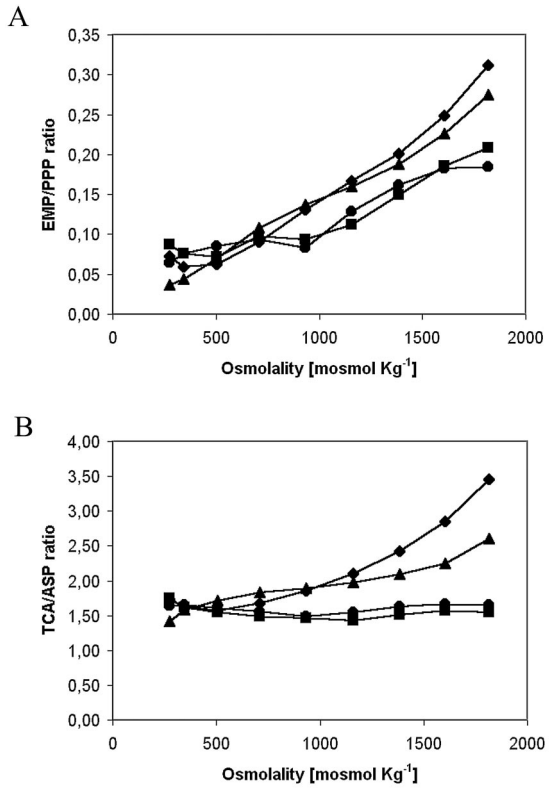

FIG. 3. Effect of rises in medium osmolality on the ratios between the main exit branches of the principal nodes at different dilution rates. (A) Glycolysis (EMP)/pentose phosphate pathway (PPP) ratio (G6P node). (B) Tricarboxylic acid cycle (TCA)/aspartate synthesis (ASP) ratio (OAA node). The graphs show data for 0.09 h^{-1} (circles), 0.13 h^{-1} (squares), 0.17 h^{-1} (triangles), and 0.21 h^{-1} (diamonds).

visiae (3, 30). The protective role of trehalose against these stress conditions requires the presence of trehalose on both sides of the membrane (3). This could explain the slight increase in the specific net excretion rate of trehalose with increases in osmotic pressure. Another possibility that cannot be excluded is the release of trehalose from corynomycolates during mycolic acid assembly at the cell wall (25). This would also result in an increase in the extracellular concentration of trehalose.

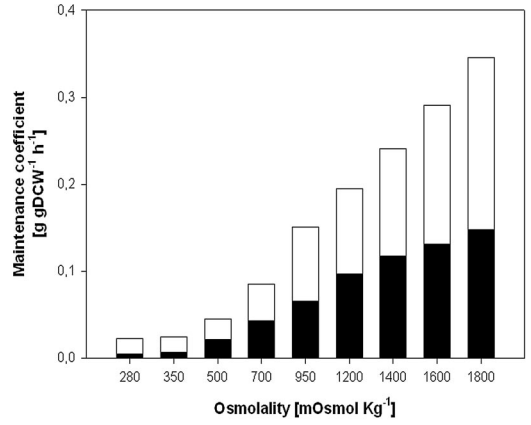

FIG. 4. Effect of medium osmolality on cell maintenance. The bars indicate the specific maintenance coefficients for cellular integrity (m_s [black]) and for cellular productivity (m_{sp} [white]).

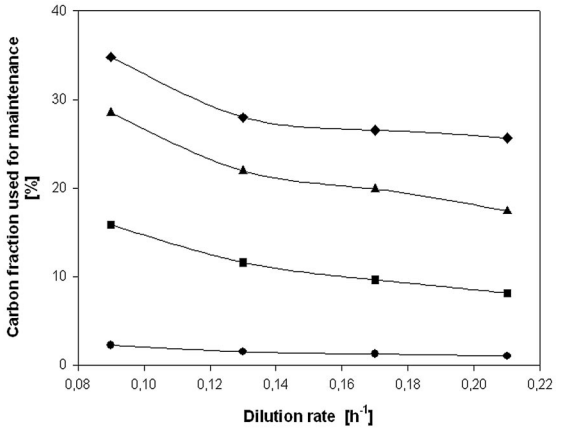

FIG. 5. Effect of dilution rate on the amount of carbon flux employed for maintenance at the following osmolalities: 280 (circles), 700 (squares), 1,200 (triangles), and 1,800 (diamonds) mosmol kg^{-1}.

Depending on the dilution rate, higher osmotic pressures prompted different flux distribution responses. At a dilution rate of 0.09 h^{-1}, most of the fluxes in the metabolic network increased. The distribution of metabolic fluxes changed at 0.21 h^{-1}, however. By redistributing the fluxes used for energy production (glycolysis and the Krebs cycle), cells growing at 0.21 h^{-1} adapted better to high osmotic pressures.

Within the metabolic network, the OAA node is directly involved in generating energy since the fluxes exiting the node determine the carbon fraction used for energy formation through the Krebs cycle and for lysine production. At high dilution rates, the OAA node was flexible. This adaptability to changes in osmotic pressure improves the cell's energy management efficiency, as at low dilution rates we found the node to be rigid. High dilution rates trigger a metabolic switch within *C. glutamicum*, which improves the cell's chances for surviving the adverse conditions of rising osmolality. For industrial applications in which the osmotic pressure increases during the course of production, the dilution rate should be kept low (taking advantage of the rigid node) to retain cell productivity.

At high osmotic pressures, while the biomass formation rate fell, the substrate consumption and CO_2 production rates increased. Therefore, additional carbon and energy are required to sustain microbial metabolism under osmotic stress (18). The carbon fraction used for maintenance increased at lower dilution rates given the same osmolality, which is indicative of an inverse relationship between the substrate and energy requirements and the rate of dilution (17). At 0.09 h^{-1}, this fraction increased 15-fold, while at 0.21 h^{-1}, it rose 25-fold. Since cells are better adapted to rises in osmolality at the latter dilution rate, an energetic redistribution is critical for coping with these stress conditions.

Independent of the rate of dilution, the ratio of the maintenance of cellular integrity (m_s) to the maintenance of cellular productivity (m_{sp}) increased as the osmolality rose. In other words, cellular integrity is always a priority over the energy and carbon needs for production. Hence, an upshift in osmolality

increases the maintenance requirements for sustaining cell integrity and significantly reduces productivity, as the microorganism needs more energy to adapt to a continuously changing environment.

In response to high osmotic pressure, the fivefold rise in the ATP maintenance coefficient reflected the higher energy demands to form and sustain ionic gradients across the cell membrane and to counteract ion diffusion into the cytoplasm (19). The ATP content has been observed to increase under conditions of osmotic stress (15, 16), but this is the first quantification of the coefficient. It is now possible to determine how many ATP moles are necessary to sustain 1 g of biomass as the osmolality rises.

In conclusion, the cell undergoes metabolic changes to cope with a demand for energy as osmotic pressure rises in the extracellular medium. Thus, a modified energetic balance impacts biomass formation and productivity, since cells use carbon and energy sources to sustain viability, favoring homeostasis over growth. Energy pool management is the cell's top priority under stress conditions.

APPENDIX A

The following are biochemical reactions and metabolites used for the construction of the *C. glutamicum* ATCC 21253 stoichiometric model.

PEP-glucose phosphotransferase system

$$\text{Glucose} + \text{Phosphoenolpyruvate} \rightarrow \text{Glucose-6P} + \text{Pyruvate}_{IN} \quad \text{(A1)}$$

Trehalose synthesis

$$2\ \text{Glucose-6P} + \text{ATP} \rightarrow \text{Trehalose}_{IN} + \text{ADP} \quad \text{(A2)}$$

Embden Meyerhof-Parnas Pathway

$$\text{Glucose-6P} \rightarrow \text{Fructose-6P} \quad \text{(A3)}$$

$$\text{Fructose-6P} + \text{ATP} \rightarrow 2\ \text{Glyceraldehyde-3P} + \text{ADP} \quad \text{(A4)}$$

$$\text{Glyceraldehyde-3P} + \text{ADP} + \text{NAD} \rightarrow \text{NADH} + \text{3-Phosphoglycerate} + \text{ATP} \quad \text{(A5)}$$

$$\text{3-Phosphoglycerate} \rightarrow \text{Phosphoenolpyruvate} + H_2O \quad \text{(A6)}$$

$$\text{Phosphoenolpyruvate} + \text{ADP} \rightarrow \text{ATP} + \text{Pyruvate}_{IN} \quad \text{(A7)}$$

$$\text{Pyruvate}_{IN} + \text{NADH} \rightarrow \text{Lactate}_{IN} + \text{NAD} \quad \text{(A8)}$$

Anaplerotic reactions (pyruvate carboxylase)

$$\text{Pyruvate}_{IN} + CO_2 + \text{ATP} + H_2O \rightarrow \text{Oxaloacetate} + \text{ADP} \quad \text{(A9)}$$

Tricarboxylic acid cycle

$$\text{Pyruvate}_{IN} + \text{COA} + \text{NAD} \rightarrow \text{Acetyl-CoA} + CO_2 + \text{NADH} \quad \text{(A10)}$$

$$\text{Acetyl-CoA} + \text{Oxaloacetate} + H_2O \rightarrow \text{Isocitrate} + \text{CoA} \quad \text{(A11)}$$

$$\text{Isocitrate} + \text{NADP} \rightarrow \alpha\text{-Ketoglutarate} + \text{NADPH} + CO_2 \quad \text{(A12)}$$

$$\alpha\text{-Ketoglutarate} + \text{CoA} + \text{NAD} \rightarrow \text{Succinyl-CoA} + CO_2 + \text{NADH} \quad \text{(A13)}$$

$$\text{Succinyl-CoA} + \text{ADP} \rightarrow \text{Succinate} + \text{CoA} + \text{ATP} \quad \text{(A14)}$$

$$\text{Succinate} + H_2O + \text{FAD} \rightarrow \text{Malate} + \text{FADH} \quad \text{(A15)}$$

$$\text{Malate} + \text{NAD} \rightarrow \text{Oxaloacetate} + \text{NADH} \quad \text{(A16)}$$

Acetate production

$$\text{Acetyl-CoA} + \text{ADP} \rightarrow \text{Acetate}_{IN} + \text{CoA} + \text{ATP} \quad \text{(A17)}$$

Glutamate, glutamine, alanine, valine, and proline production

$$NH_3 + \alpha\text{-Ketoglutarate} + \text{NADPH} \rightarrow \text{Glutamate}_{IN} + H_2O + \text{NADP} \quad \text{(A18)}$$

$$\text{Glutamate}_{IN} + NH_3 + \text{ATP} \rightarrow \text{Glutamine}_{IN} + \text{ADP} \quad \text{(A19)}$$

$$\text{Pyruvate}_{IN} + \text{Glutamate}_{IN} \rightarrow \text{Alanine}_{IN} + \alpha\text{-Ketoglutarate} \quad \text{(A20)}$$

$$2\ \text{Pyruvate}_{IN} + \text{NADPH} + \text{Glutamate}_{IN} \rightarrow \text{Valine}_{IN} + CO_2 + H_2O + \text{NADP} + \alpha\text{-Ketoglutarate} \quad \text{(A21)}$$

$$\text{Glutamate}_{IN} + \text{ATP} + 2\ \text{NADPH} \rightarrow \text{Proline}_{IN} + \text{ADP} + 2\ \text{NADP} \quad \text{(A22)}$$

Pentose phosphate cycle

$$\text{Glucose-6P} + H_2O + 2\ \text{NADP} \rightarrow \text{Ribulose-5P} + CO_2 + 2\ \text{NADPH} \quad \text{(A23)}$$

$$\text{Ribulose-5P} \rightarrow \text{Ribose-5P} \quad \text{(A24)}$$

$$\text{Ribulose-5P} \rightarrow \text{Xylulose-5P} \quad \text{(A25)}$$

$$\text{Xylulose-5P} + \text{Ribose-5P} \rightarrow \text{Sedoheptulose-7P} + \text{Glyceraldehyde-3P} \quad \text{(A26)}$$

$$\text{Sedoheptulose-7P} + \text{Glyceraldehyde-3P} \rightarrow \text{Fructose-6P} + \text{Erythrose-4P} \quad \text{(A27)}$$

$$\text{Xylulose-5P} + \text{Erythrose-4P} \rightarrow \text{Fructose-6P} + \text{Glyceraldehyde-3P} \quad \text{(A28)}$$

Oxidative phosphorylation P/O=2

$$2\ \text{NADH} + O_2 + 4\ \text{ADP} \rightarrow 2\ H_2O + 4\ \text{ATP} + 2\ \text{NAD} \quad \text{(A29)}$$

$$2\ FADH + O_2 + 2\ ADP \rightarrow 2\ H_2O + 2\ ATP + 2\ FAD \quad (A30)$$

Aspartate and lysine production

$$Oxaloacetate + Glutamate_{IN} \rightarrow Aspartate_{IN} + \alpha\text{-Ketoglutarate} \quad (A31)$$

$$Aspartate_{IN} + Pyruvate_{IN} + 2\ NADPH + Succinyl\text{-}CoA + Glutamate_{IN} + ATP \rightarrow Succinate + \alpha\text{-Ketoglutarate} + CO_2 + Lysine_{IN} + 2\ NADP + CoA + ADP \quad (A32)$$

Biomass synthesis

$$0.012\ Glucose\text{-}6P + 0.041\ Fructose\text{-}6P + 0.025\ Ribose\text{-}5P + 0.020\ Erythrose\text{-}4P + 0.030\ Glyceraldehyde\text{-}3P + 0.089\ 3\text{-}Phosphoglycerate + 0.057\ Phosphoenolpyruvate + 0.058\ Pyruvate_{IN} + 0.329\ Acetyl\text{-}CoA + 0.045\ Oxaloacetate + 0.018\ Aspartate_{IN} + 0.017\ Lysine_{IN} + 0.049\ Glutamine_{IN} + 0.073\ Alanine_{IN} + 0.026\ Valine_{IN} + 0.015\ Proline_{IN} + 0.881\ NADPH + 0.156\ NAD + 0.487\ Glutamate_{IN} + 2.930\ ATP \rightarrow Biomass + 0.017\ CO_2 + 0.489\ \alpha\text{-Ketoglutarate} + 2.930\ ADP + 0.329\ CoA + 0.881\ NADP + 0.156\ NADH \quad (A33)$$

Transport reactions

$$Trehalose_{IN} \rightarrow Trehalose_{EX} \quad (A34)$$

$$Pyruvate_{IN} \rightarrow Pyruvate_{EX} \quad (A35)$$

$$Lactate_{IN} \rightarrow Lactate_{EX} \quad (A36)$$

$$Acetate_{IN} \rightarrow Acetate_{EX} \quad (A37)$$

$$Aspartate_{IN} \rightarrow Aspartate_{EX} \quad (A38)$$

$$Glutamate_{IN} \rightarrow Glutamate_{EX} \quad (A39)$$

$$Glutamine_{IN} \rightarrow Glutamine_{EX} \quad (A40)$$

$$Proline_{IN} \rightarrow Proline_{EX} \quad (A41)$$

$$Valine_{IN} \rightarrow Valine_{EX} \quad (A42)$$

$$Lysine_{IN} \rightarrow Lysine_{EX} \quad (A43)$$

$$Alanine_{IN} \rightarrow Alanine_{EX} \quad (A44)$$

ATP dissipation reaction

$$ATP \rightarrow ADP \quad (A45)$$

The subindexes IN and EX correspond to intra- and extracellular metabolites, respectively.

APPENDIX B

The following equations were used to calculate the maintenance coefficient on a substrate, corrected for product formation.

$$r_s = Y^{\circ}_{xs}{}'\mu + m_s'$$

where the maintenance coefficient (m_s') and maximum biomass yield ($Y^{\circ}_{xs}{}'$), uncorrected for production formation, are defined as follows:

$$m_s' = m_s + (a/Y^{\circ}_{ps}) \text{ and } Y^{\circ}_{xs}{}' = (1/Y^{\circ}_{xs}) + (b/Y^{\circ}_{ps})$$

REFERENCES

1. **Bott, M., and A. Niebisch.** 2003. The respiratory chain of *Corynebacterium glutamicum.* J. Biotechnol. **104:**129–153.
2. **Ciulla, R., and M. Roberts.** 1999. Effects of osmotic stress on *Methanococcus thermolithotrophicus*: 13C-edited 1H-NMR studies of osmolyte turnover. Biochim. Biophys. Acta **1427:**193–204.
3. **Cuber, R., E. Eleutherio, M. Pereira, and A. Panek.** 1997. The role of the trehalose transporter during germination. Biochim. Biophys. Acta **1330:**165–171.
4. **Dauner, M., T. Storni, and U. Sauer.** 2001. *Bacillus subtilis* metabolism and energetics in carbon-limited and excess-carbon chemostat culture. J. Bacteriol. **183:**7308–7317.
5. **Eggeling, L., H. Sahm, and A. de Graaf.** 1996. Quantifying and directing metabolite flux: application to amino acid overproduction. Adv. Biochem. Eng. Biotechnol. **54:**1–30.
6. **Farwick, M., R. Siewe, and R. Kramer.** 1995. Glycine betaine uptake after hyperosmotic shift in *Corynebacterium glutamicum.* J. Bacteriol. **177:**4690–4695.
7. **Frings, E., H. Kunte, and E. Galinski.** 1993. Compatible solutes in representatives of the genera *Brevibacterium* and *Corynebacterium*: occurrence of tetrahydropyrimidines and glutamamine. FEMS Microbiol. Lett. **109:**25–32.
8. **González-Sepúlveda, M., and E. Agosin.** 2000. Capture of volatile metabolites for tracking the evolution of gibberellic acid in a solid-state culture of *Gibberella fujikuroi.* Biotechnol. Lett. **22:**1849–1854.
9. **Guillouet, S., and J. Engasser.** 1995. Growth of *Corynebacterium glutamicum* in glucose-limited continuous cultures under high osmotic pressure. Influence of growth rate on the intracellular accumulation of proline, glutamate and trehalose. Appl. Microbiol. Biotechnol. **44:**496–500.
10. **Guillouet, S., and J. Engasser.** 1995. Sodium and proline accumulation in *Corynebacterium glutamicum* as a response to an osmotic saline upshock. Appl. Microbiol. Biotechnol. **43:**315–320.
11. **Kiss, R., and G. Stephanopoulos.** 1992. Culture instability of auxotrophic amino-acid producers. Biotechnol. Bioeng. **40:**75–85.
12. **Kiss, R., and G. Stephanopoulos.** 1992. Metabolic characterization of an L-lysine-producing strain by continuous culture. Biotechnol. Bioeng. **39:**565–574.
13. **Lapujade, P., J. Goergen, and J. Engasser.** 1999. Glutamate excretion as a major kinetic bottleneck for the thermally triggered production of glutamic acid by *Corynebacterium glutamicum.* Metab. Eng. **1:**255–261.
14. **Martin, D., R. Ciulla, P. Robinson, and M. Roberts.** 2000. Switching osmolyte strategies: response of *Methanococcus thermalithotrophicus* to changes in external NaCl. Biochim. Biophys. Acta **1524:**1–10.
15. **Ohwada, T., and S. Sagisaka.** 1987. An immediate and steep increase in ATP concentration in response to reduced turgor pressure in *Escherichia coli* B. Arch. Biochem. Biophys. **259:**157–163.
16. **Ohwada, T., S. Sagisaka, and T. Sato.** 1994. An exclusive increase in the concentration of ATP as a result of osmotic stress in *Escherichia coli* B. Biosci. Biotechnol. Biochem. **58:**1512–1513.
17. **Oliveira, E., J. Morais, and N. Pereira.** 1992. Determination of the energy maintenance coefficient of *Zymomonas mobilis.* Biotechnol. Lett. **14:**1081–1084.
18. **Olz, R., K. Larsson, L. Adler, and L. Gustafsson.** 1993. Energy flux and osmoregulation of *Saccharomyces cerevisiae* grown in chemostats under NaCl stress. J. Bacteriol. **175:**2205–2213.
19. **Oren, A.** 1999. Bioenergetic aspects of halophilism. Microbiology and molecular biology reviews. Microbiol. Mol. Biol. Rev. **63:**334–348.
20. **Petersen, S., A. de Graaf, L. Eggeling, M. Mollney, W. Wiechert, and H. Sahm.** 2000. In vivo quantification of parallel and bidirectional fluxes in the anaplerosis of *Corynebacterium glutamicum.* J. Biol. Chem. **275:**35932–35941.
21. **Peter-Wendisch, P., V. Wendisch, S. Paul, B. Eikmanns, and H. Sahm.** 1997. Pyruvate carboxylase as an anaplerotic enzyme in *Corynebacterium glutamicum.* Microbiology **143:**1095–1103.
22. **Pons, A., C. Dussap, C. Péquignot, and J. Gros.** 1996. Metabolic flux distribution in *Corynebacterium melassecola* ATCC 17965 for various carbon sources. Biotechnol. Bioeng. **51:**177–189.
23. **Regev, R., I. Peri, H. Gilboa, and Y. Avi-Dor.** 1990. 13C NMR study of the interrelation between synthesis and uptake of compatible solutes in two moderately halophilic eubacteria, bacterium Ba1 and *Vibrio costicola.* Arch. Biochem. Biophys. **278:**106–112.
24. **Russell, J., and G. Cook.** 1995. Energetics of bacterial growth: balance of anabolic and catabolic reactions. Microbiol. Rev. **59:**48–62.
25. **Shimakata, T., and Y. Minatogawa.** 2000. Essential role of trehalose in the synthesis and subsequent metabolism of corynomycolic acid in *Corynebacterium matruchotii.* Arch. Biochem. Biophys. **380:**331–338.
26. **Skjerdal, O., H. Sletta, S. Flenstad, K. Josefsen, D. Levine, and T. Ellingsen.** 1995. Changes in cell volume, growth and respiration rate in response to hyperosmotic stress of NaCl, sucrose and glutamic acid in *Brevibacterium lactofermentum* and *Corynebacterium glutamicum.* Appl. Microbiol. Biotechnol. **43:**1099–1106.

27. **Stephanopoulos, G., A. Aristidou, and J. Nielsen.** 1998. Metabolic engineering: principles and methodologies. Academic Press, San Diego, Calif.
28. **Stephanopoulos, G., and J. Vallino.** 1991. Network rigidity and metabolic engineering in metabolite overproduction. Science **252:**1675–1681.
29. **Stouthamer, A., and H. van Verseveld.** 1987. Microbial energetics should be considered in manipulating metabolism for biotechnological purposes. TIBTECH **5:**149–156.
30. **Styrvold, O., and A. Strom.** 1991. Synthesis, accumulation, and excretion of trehalose in osmotically stressed *Escherichia coli* K-12 strains: influence of amber suppressors and function of the periplasmic trehalase. J. Bacteriol. **173:**1187–1192.
31. **Takiguchi, N., H. Shimizu, and S. Shioya.** 1997. An online physiological-state recognition system for the lysine fermentation process based on a metabolic reaction model. Biotechnol. Bioeng. **55:**170–181.
32. **Vallino, J., and G. Stephanopoulos.** 1994. Carbon flux distributions at the glucose-6-phosphate branch point in *Corynebacterium glutamicum* during lysine overproduction. Biotechnol. Prog. **10:**327–334.
33. **Vallino, J., and G. Stephanopoulos.** 1993. Metabolic flux distributions in *Corynebacterium glutamicum* during growth and lysine overproduction. Biotechnol. Bioeng. **41:**633–646.
34. **Varela, C., E. Agosin, M. Baez, M. Klapa, and G. Stephanopoulos.** 2003. Metabolic flux redistribution in *Corynebacterium glutamicum* in response to osmotic stress. Appl. Microbiol. Biotechnol. **60:**547–555.
35. **Ventosa, A., J. Nieto, and A. Oren.** 1998. Biology of moderately halophilic aerobic bacteria. Microbiol. Mol. Biol. Rev. **62:**504–544.